ICAS 2021 SHANG HAI
32nd Congress of the International Council of the Aeronautical Sciences
September 6-10, 2021 Pudong Shangri-La, Shanghai, China

Virtual Flight Test of a BWB Aircraft in Low Speed Wind Tunnel

Bowen NIE [1], Fei CEN [1], Zhitao LIU [1*], Tianhao GUO [1] & Haisheng SUN [1]

[1] Low Speed Aerodynamics Institute, China Aerodynamics Research and Development Center, Mianyang 621000, China

Abstract

This paper summarizes the virtual flight test of a Blended-Wing-Body(BWB) aircraft model in the wind tunnel at the Low Speed Aeronautics Institution (LSAI) of the China Aerodynamics Research and Development Center (CARDC). The virtual flight test mainly aims to validate and evaluate the flight control laws using dynamical sub-scaled aircraft model, which is equipped with the flight control system. First, the overview of the BWB aircraft model is briefly introduced, including the criteria of dynamic similarity, the physical properties, the onboard sensors and actuators. Second, Modeling of the BWB aircraft is presented in detail, especially for the aerodynamic forces and moments resulting from the tabulate and interpolation of wind tunnel test data. Third, a Control Augmentation System (CAS) is designed with the classical flight control technique assuming that the coupling between the longitudinal and lateral/directional channel is negligible. Finally, the effectiveness and performance of the CAS is preliminarily demonstrated via simulations, and then a series of virtual flight tests are carried out to validate and evaluate the close-loop performances via pilot steering and standard maneuvers.

Keywords: Blended-Wing-Body, aerodynamic modeling, control augmentation system, virtual flight test

1. Introduction

The BWB configuration is a promising candidate of the future civil aircraft due to the significant reduction of fuel consumption and noise emission[1]. Compared to the conventional aircrafts, the fuselage of BWB configuration is flattened and smoothly blended into the wing for higher lift contribution and reduced wetted area. As a result, the cruise lift-to-drag ratio of BWB configuration is potentially improved to be 120% of the equivalent conventional one[2,3]. Besides, the BWB configuration is beneficial for noise shielding due to the feasible engine integration on top of the fuselage[4,5].

However, the design of BWB configuration is quite challenging in the aspect of flying properties and controllability[6]. To explore the potential performance, the BWB aircraft does not necessarily to have be designed to be inherently stable. In general, the BWB aircraft features a weak directional stability and a limited yaw damping. Especially for the case of tailless, the BWB aircraft always suffers from the lack of vertical and horizontal tails, and small static margin is often required to obtain sufficient pitch control authority. Therefore, a flight control system is normally required to stabilize the BWB aircraft and provide the satisfiable handling qualities[7,8]. Since the aerodynamic layout affects the flight dynamics drastically, control law validation and handling qualities assessment of BWB aircraft in the preliminary design phase require particular attention[9].

The technique of flight tests in the wind tunnel has been developed and applied to validate the flight control scheme and evaluate the closed-loop performance of the BWB aircrafts. In the Langley Full-Scale Tunnel (LFST), successful free flights had been performed for a 5% sub-scaled BWB aircraft, and satisfiable performances of stability augmentation and surface allocation are achieved[10]. In the L2000 wind tunnel of the Royal Institute of Technology, a BWB configuration named Swing was supported with an one degree-of-freedom(DOF) rig for investigation of yaw departure and recovery, and a dynamic-recovery scheme was developed and implemented to address the issue of insufficient split-flap effectiveness at large sideslip[11,12]. In the FL-14 wind tunnel of the CARDC, the technique of virtual flight test has been developed based on a 3-DOF rig, which is actually a pilot-in-the-loop(PIL) experimental setup and is adequate for validation and evaluation of the BWB aircraft model[13].

In this paper, the stability and controllability of a sub-scaled BWB aircraft is concerned. Based on the

flight dynamics model, a control augmentation system(CAS) is developed to stabilize the attitude and improve the flying and handling qualities. The performance of the closed-loop system is validated and evaluated via a series of virtual flight tests. This paper is organized as follows. The mathematical model is described in section 2. The flight control law is given in section 3. The virtual flight tests and typical results are presented in section 4. Finally, section 5 concludes the paper.

2. Modeling of the BWB Aircraft

2.1 Overview of the BWB Model

As illustrated in Figure 1, a 10% dynamically sub-scaled model of the BWB aircraft is designed and fabricated to fulfill the geometry, mass, inertia and thrust similarity criteria[13] in eq.(1).

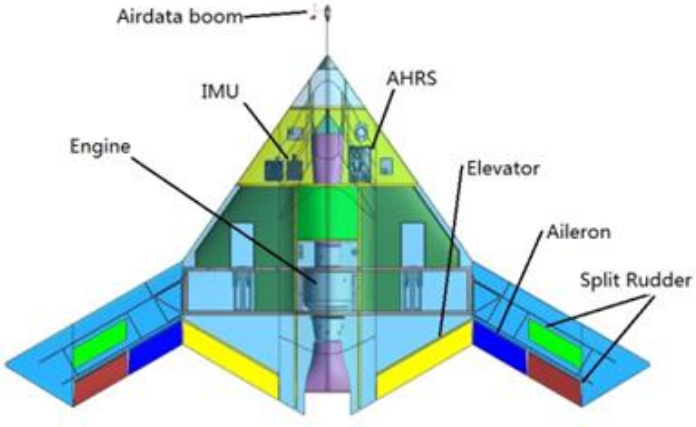

Figure 1 – Layout of the BWB aircraft Model.

$$\begin{cases} \dfrac{V_f^2}{g_f l_f} = \dfrac{V_m^2}{g_m l_m} & (Fr\ similarity) \\ \dfrac{m_f}{l_f^3 \rho_f} = \dfrac{m_m}{l_m^3 \rho_m} & (mass\ similarity) \\ \dfrac{J_f}{l_f^5 \rho_f} = \dfrac{J_m}{l_m^5 \rho_m} & (inertia\ similarity) \\ \dfrac{T_f}{m_f g_f} = \dfrac{T_m}{m_m g_m} & (thrust\ similarity) \end{cases} \tag{1}$$

Where V is the airspeed, m is the mass, J is the inertia, T is the engine thrust, g is the gravity coefficient, l is the characteristic length, ρ is the air density, and the subscript f and m represent the full-scale aircraft and the sub-scale model respectively.

To save weight and space for the onboard devices, the fuselage and wing is mainly constructed with metal skeleton and carbon fiber skin. The key physical parameters are carefully conditioned and listed in Table 1.

Table 1 – Physical properties of the dynamically scaled BWB model.

Item	Symbol	Value
Scale ratio	K	10%
Span	b	2.0 m
Mean chord	$\bar{c}$	0.6571 m
Wing area	S	0.8742 m^2
Mass	m	16.85 kg
Moment of inertia	$J_X / J_Y / J_Z$	1.1017/ 0.7380/ 1.6920 $kg.m^2$

There are eight control surfaces, each driven by a servo actuator, which can be allocated to the conventional elevator δ_e, aileron δ_a and rudder δ_r as presented in Table 2. Besides, the left and right wing tips are also able to rotate symmetrically to change the airframe configuration. To be mentioned is that the Split-Drag-Rudder(SDR) is composed of two spoils, one in the mid and the other on the trailing edge of each wing. Sensors are attached to the fuselage and aligned with the body axes, including the Air data boom (vane for AOA/AOS - angle of attack/sideslip), the IMU (Inertial Measurement Unit) for angular rates & linear accelerometers and the AHRS (Attitude and Heading Reference System) for attitude angles. The dynamic pressure and air speed is set and controlled by the wind tunnel.

Table 2 – Deflection range of the surfaces on the BWB aircraft.

Surface	Notation	Position Bound	Rate Limit
Aileron / Elevator	δ_a / δ_e	±30°	±200 °/s
Rudder	δ_r	±40°	±200 °/s
Wingtip	δ_{wt}	±40°	±200 °/s

2.2 Equations of Motion

The BWB aircraft motion can be represented with the general 12th order model, including the dynamics, kinematics and navigation equations[14]:

$$\begin{cases} \dot{\vec{V}} = \dfrac{F}{m} - \vec{\Omega} \times \vec{V} \\ \dot{\vec{\Omega}} = I^{-1}\left(M - \vec{\Omega} \times I\vec{\Omega}\right) \\ \dot{\Phi} = T\left(\Phi\right)\vec{\Omega} \\ \dot{X} = R\left(\Phi\right)V \end{cases} \tag{2}$$

Where $\vec{V} = [u, v, w]^T$ and $\vec{\Omega} = [p, q, r]^T$ denote the translational and angular velocity vector in the body-axis frame respectively, $\Phi = [\phi, \theta, \psi]^T$ represents the Euler's angles, $X = [x, y, z]^T$ is the position of the center of gravity(CG). The transformation matrix and rotation matrix are given as:

$$T\left(\Phi\right) = \begin{bmatrix} 1 & \sin\phi\tan\theta & \cos\phi\tan\theta \\ 0 & \cos\phi & -\sin\phi \\ 0 & \sin\phi/\cos\theta & \cos\phi/\cos\theta \end{bmatrix} \tag{3}$$

$$R\left(\Phi\right) = \begin{bmatrix} \cos\theta\cos\psi & \sin\phi\sin\theta\cos\psi - \cos\phi\sin\psi & \cos\phi\sin\theta\cos\psi + \sin\phi\sin\psi \\ \cos\theta\sin\psi & \sin\phi\sin\theta\sin\psi + \cos\phi\cos\psi & \cos\phi\sin\theta\sin\psi - \sin\phi\cos\psi \\ -\sin\theta & \sin\phi\cos\theta & \cos\phi\cos\theta \end{bmatrix} \tag{4}$$

The forces applied to the BWB aircraft can be decomposed into three terms, including the aerodynamic forces, engine thrust and gravity. The moments about the aircraft CG result from the aerodynamic actions and engine thrust.

$$F = F_{aero} + F_{engine} + F_{gravity} \tag{5}$$

$$M = M_{aero} + M_{engine} \tag{6}$$

The aerodynamic forces expressed in the body-axis are obtained as:

$$F_a = \bar{q}S \begin{bmatrix} -\cos\alpha & 0 & \sin\alpha \\ 0 & 1 & 0 \\ -\sin\alpha & 0 & -\cos\alpha \end{bmatrix} \begin{bmatrix} C_D \\ C_Y \\ C_L \end{bmatrix} \tag{7}$$

$$M_a = \bar{q}S\begin{bmatrix} b\cdot C_l \\ \bar{c}\cdot C_m \\ b\cdot C_n \end{bmatrix} + \overrightarrow{GA}\times F_a \tag{8}$$

where C_D, C_Y, C_L is the aerodynamic force coefficient of drag, side force and lift; C_l, C_m, C_n denote the aerodynamic moment coefficient of roll, pitch and yaw; $\bar{q} = \frac{1}{2}\rho V^2$ is the air dynamic pressure; α is the angle of attack; $\overrightarrow{GA} = [\Delta x, \Delta y, \Delta z]^T$ refers to the misalignment between the aerodynamic applied point and the CG.

It is reasonable to assume that the engine thrust is alignment with the longitudinal body axis. As a result the forces and moments resulting from the engine are:

$$F_{engine} = \begin{bmatrix} T_e \\ 0 \\ 0 \end{bmatrix} \tag{9}$$

$$M_{engine} = \begin{bmatrix} 0 \\ z_{engine}\cdot T_e \\ 0 \end{bmatrix} \tag{10}$$

where z_{engine} is the vertical shift between the engine and the aircraft CG.

The gravity forces, projected in the body-axis frame, are given by:

$$F_{gravity} = mg\begin{bmatrix} -\sin\theta \\ \cos\theta\sin\phi \\ \cos\theta\cos\phi \end{bmatrix} \tag{11}$$

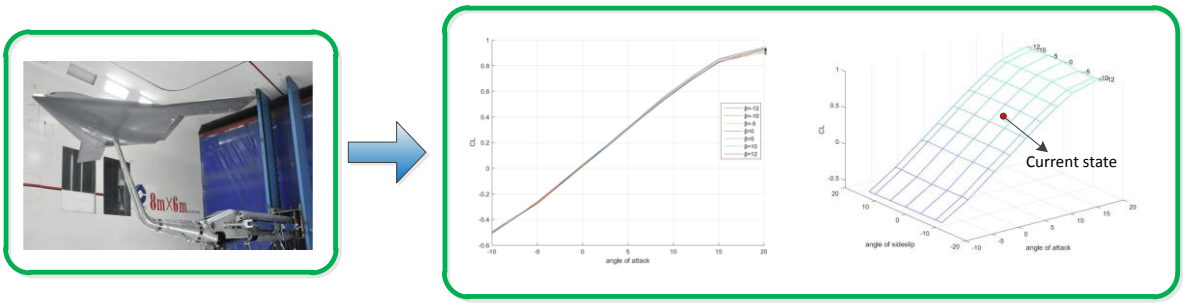

Figure 2 – Aerodynamic test and modeling.

As shown in Fig.2, all the coefficients in eq. (7) and eq. (8) are evaluated from the static wind tunnel tests and dynamic forced oscillation tests. Each term in the aerodynamic model has a database that is arranged in an n-dimensional lookup table, where n is equal to the number of independent variables as following:

$$C_D = C_{D0}(\alpha,\beta) + \Delta C_{D_{\delta_e}}(\alpha,\delta_e) + \Delta C_{D_{\delta_a}}(\alpha,\beta,\delta_a) + \Delta C_{D_{\delta_r}}(\alpha,\beta,\delta_r) \tag{12}$$

$$C_Y = C_{Y0}(\alpha,\beta) + \Delta C_{Y_{\delta_a}}(\alpha,\beta,\delta_a) + \Delta C_{Y_{\delta_r}}(\alpha,\beta,\delta_r) \tag{13}$$

$$C_L = C_{L0}(\alpha,\beta) + \Delta C_{L_{\delta_e}}(\alpha,\delta_e) + \Delta C_{L_{\delta_a}}(\alpha,\beta,\delta_a) + \Delta C_{L_{\delta_r}}(\alpha,\beta,\delta_r) \tag{14}$$

$$C_l = C_{l0}(\alpha,\beta) + \Delta C_{l_{\delta_a}}(\alpha,\beta,\delta_a) + \Delta C_{l_{\delta_r}}(\alpha,\beta,\delta_r) + \hat{C}_{l_p}(\alpha)\hat{p} + \hat{C}_{l_r}(\alpha)\hat{r} \tag{15}$$

$$C_m = C_{m0}(\alpha) + \Delta C_{m_{\delta_e}}(\alpha,\delta_e) + \hat{C}_{m_q}(\alpha)\hat{q} \tag{16}$$

$$C_n = C_{n0}(\alpha,\beta) + \Delta C_{n_{\delta_a}}(\alpha,\beta,\delta_a) + \Delta C_{n_{\delta_r}}(\alpha,\beta,\delta_r) + \hat{C}_{n_p}(\alpha)\hat{p} + \hat{C}_{n_r}(\alpha)\hat{r} \tag{17}$$

where β is the angle of sideslip; the normalized rotation rates are defined as $\hat{p} = pb/2V$,

$\hat{q} = q\bar{c}/2V$, $\hat{r} = rb/2V$.

3. Flight Control Law Design

3.1 Control Design Objectives

Following a standard approach, the nonlinear model of eq. (2) is trimmed to steady level flight and linearized to be linear state-space equations. For ease of control design, coupling between the longitudinal and lateral/directional channel is always neglected.

As shown in Fig. 3, the longitudinal flight dynamics of the BWB aircraft are similar to a conventional aircraft at low α. However, poles of the short period mode move to the real axis with the increase of α. In the section of $8.6° < \alpha < 10°$, the phugoid and short period mode corrupted to a third mode and two real poles, one of which locates at the right half plane.

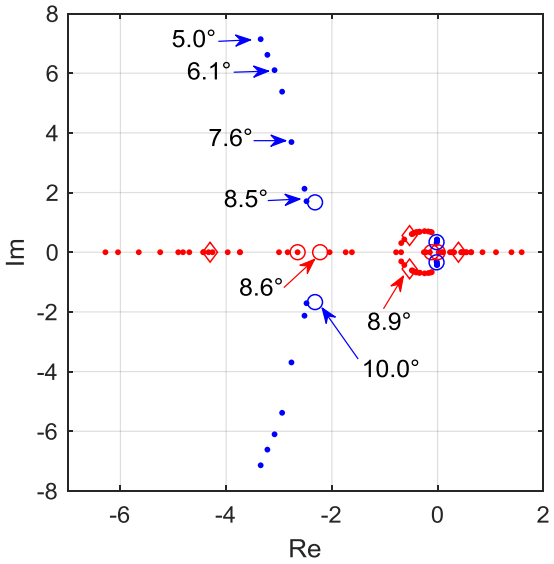

Figure 3 – Longitudinal modal characteristics.

The lateral/directional flight dynamics of the BWB aircraft are complicated, because no typical Dutch-roll mode is discovered in Fig. 4(a). It is believed that the Dutch-roll mode corrupts to two real poles due to the lack of vertical tail as presented in Fig. 4(b). Obviously, the lateral/directional channel suffers from the lack of stability or damping. Stability augmentation system(SAS) or CAS is essential to stabilize the BWB aircraft.

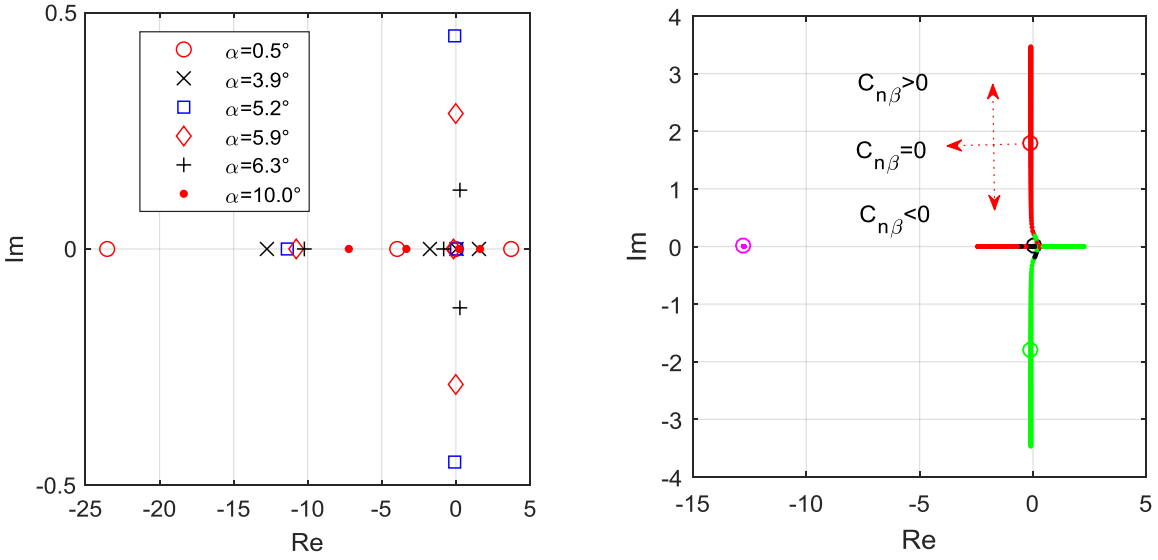

(a) Modal distribution and evolution (b) Dutch-roll mode evolution with respect to $C_{n\beta}$

Figure 4 – Lateral/directional modal characteristics.

Hence, the primary control objective is to augment the open-loop system for satisfactory closed-loop flying and handling qualities.

3.2 Control Augmentation System

3.2.1 Longitudinal Controller

Pitch rate tracking is selected for the longitudinal control architecture, giving the pilot direct command of the desired nose up or down. The architecture is composed of a SAS and a CAS as presented in Fig. 5.

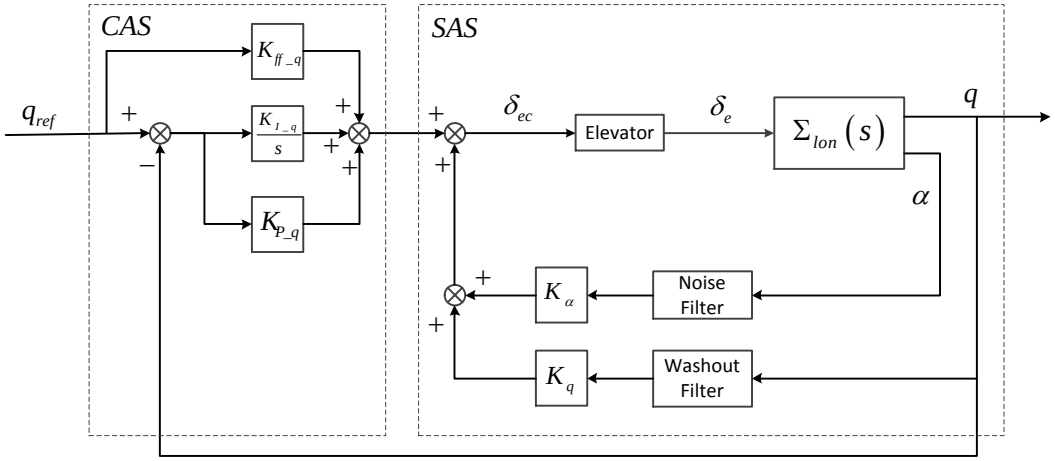

Figure 5 – Longitudinal controller architecture.

The longitudinal state-space model $\sum_{lon}(S)$ is obtained at the level flight states and given by:

$$\begin{cases} \dot{x}_{lon} = A_{lon}x_{lon} + Bu_{lon} \\ y_{lon} = C_{lon}x_{lon} \end{cases} \tag{18}$$

where $x_{lon} = [V, \alpha, q, \theta]^T$, $u_{lon} = \delta_e$, $y_{lon} = [\alpha, q]^T$.

A low-pass filter $10/(s+10)$ is applied to the α feedback to remove the high frequency noise , and a high-pass filter $s/(s+3)$ is used to washout the low frequency component of q. Taking the filters, control gains and integrator into account, the closed-loop system can be expressed as:

$$\begin{cases} \begin{bmatrix} \dot{x}_{lon} \\ \dot{x}_{qf} \\ \dot{x}_{\alpha f} \\ \dot{x}_{i\_q} \end{bmatrix} = \underbrace{\begin{bmatrix} A_{lon} + (K_q - K_{P\_q})BC_{lon}(q) & -K_qB & K_\alpha B & K_{I\_q}B \\ 3C_{lon}(q) & -3 & 0 & 0 \\ 10C_{lon}(\alpha) & 0 & -10 & 0 \\ -C_{lon}(q) & 0 & 0 & 0 \end{bmatrix}}_{A_{lon\_cl}} \begin{bmatrix} x_{lon} \\ x_{qf} \\ x_{\alpha f} \\ x_{i\_q} \end{bmatrix} + \underbrace{\begin{bmatrix} (K_{P\_q} + K_{ff\_q}) \\ 0 \\ 0 \\ 1 \end{bmatrix}}_{B_{lon\_cl}} \delta_e \\ q = \underbrace{\begin{bmatrix} C_{lon}(q) & 0 & 0 & 0 \end{bmatrix}}_{C_{lon\_cl}} \begin{bmatrix} x_{lon} \\ x_{qf} \\ x_{\alpha f} \\ x_{i\_q} \end{bmatrix} \end{cases} \tag{19}$$

where x_{qf} , $x_{\alpha f}$ and x_{i_q} is the washout filter, noise filter and integrator state respectively.

Therefore, the proportional and integral gains K_{P_q} and K_{I_q}, the feedback gains K_α and K_q, and the feedforward gain K_{ff_q} are to be optimized and scheduled to achieve good handling and flying performance at different α.

The designed longitudinal controller is applied to the nonlinear aircraft model of eq. (2). At the level flight state of $\alpha \approx 5°$, a doublet maneuver is applied to the longitudinal stick q_f at 10s. One can note that the performance of pitch rate tracking is satisfactory. Notable tracking error is observed at about

50s, 55s and 60s, which is induced by directional maneuver and suppressed by the longitudinal controller rapidly.

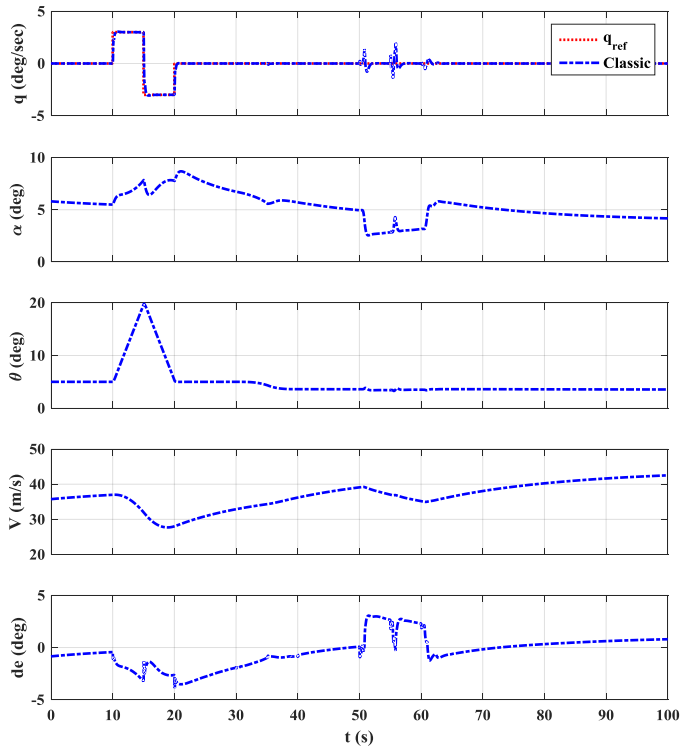

Figure 6 – Longitudinal control performance in simulation.

3.2.2 Lateral/directional Controller

Similar to the longitudinal axis, roll rate tracking is selected in the lateral channel. Sideslip angle tracking and aileron-rudder-interconnection(ARI) is required for coordinated turns and cross wind landings. The lateral/directional controller architecture is illustrated in Fig. 7. One can note that filters and integrator are also added to the lateral/directional open-loop system $\sum_{lat}(s)$, which is a four state($x_{lat}=[\beta, p, r, \phi]^T$) model with two inputs($u_{lon}=[\delta_a, \delta_r]^T$).

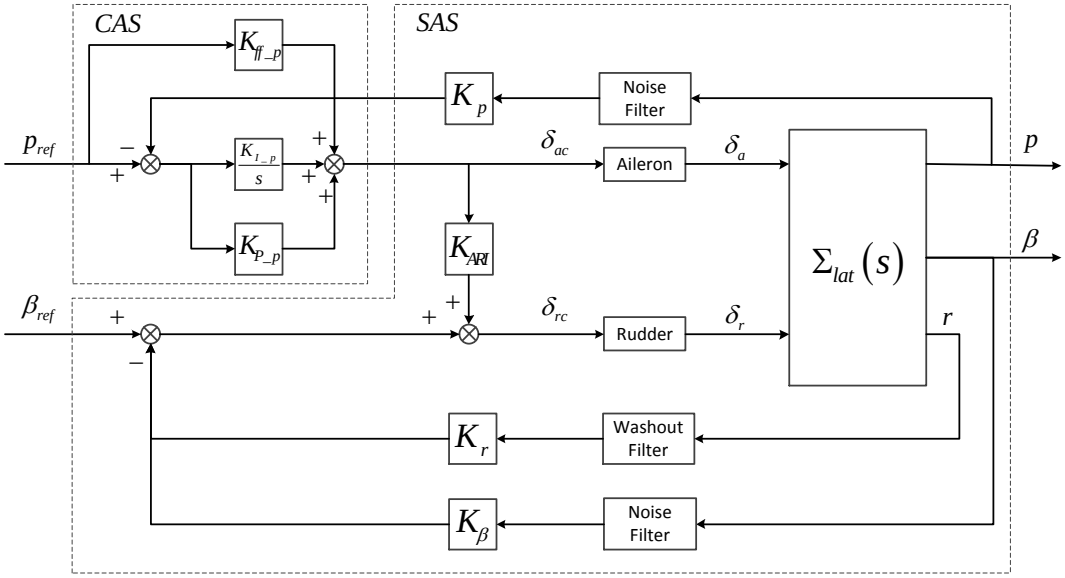

Figure 7 – Lateral/directional controller architecture.

Since significant modal variation is observed and no conventional Dutch-roll characteristics is presented in Fig. 4(a), the feedback gains of the lateral/directional controller are determined by α using the approach of gain-schedule. Closed-loop simulations are carried out to validate the performance of reference tracking and decoupling. As demonstrated in Fig. 8, the wing is held at level and the sideslip is kept at zero though significant maneuver is performed between 10s and 20s,

doublet reference command is applied to the channel of roll and yaw at 30s and 50s respectively. It is noted that the actual roll rate track the reference signal well and the ideal feature of integration is observed between the roll rate and angle. Notable tracking error is found for β, though the magnitude of overshoot, time-delay and oscillation is acceptable. Further improvement of β response is restrained by the limited yaw control effect as presented in the bottom plot of Fig. 8. When the sideslip is held at $\beta = 5°$, the deflection of rudder is required to be $\delta_r \approx 20°$. Besides, adverse coupling between the channel of roll and yaw, yaw and pitch is inevitable and acceptable.

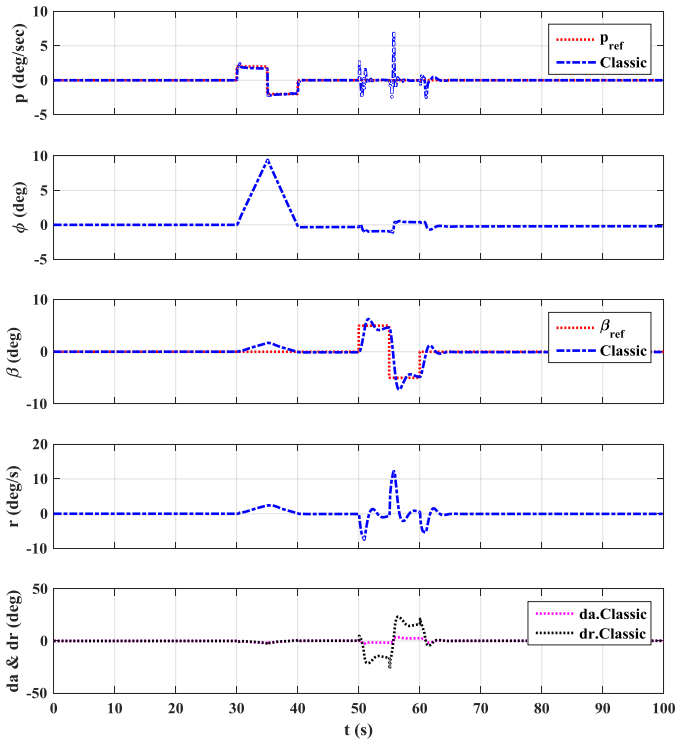

Figure 8 – Lateral/directional control performance in simulation.

4. Virtual Flight Test and Typical Results

To validate the flight control system, virtual flight tests are conducted with the 10% scaled BWB aircraft model in the wind tunnel. Conventional maneuvers over large range of alpha are conducted to demonstrate the closed-loop flying and handling performances.

4.1 Overview of the Experimental Setup

Figure 9 – Virtual flight test of the BWB model.

As shown in Fig. 9, the BWB aircraft model is supported in the wind tunnel test section by a 3-DOF rig from the bottom. A spherical joint is selected to connect the vertical sting and the aircraft model at the CG. Since the friction of the joint is negligible, the model is able to rotate freely in roll. pitch and yaw in the range of about $\pm 40°$. Moreover, the BWB model is equipped with sensors, including two vanes for α / β, an IMU for the angular rates and an AHRS for the Euler angles. Besides, each

surface is driven by a servo actuator according to the commands from the flight computer, which is placed outside the wind tunnel and wired to the onboard avionics for communication and power supply.

In the virtual flight tests, the airspeed is regulated by the wind tunnel, the aircraft model is driven by the airflow and stabilized by the surface deflections, a "pilot" is responsible to handle the aircraft with a stick and evaluate the closed-loop system via standard reference inputs.

4.2 Typical Results and Analysis

4.2.1 Pilot Steering and Evaluation

It is expected that the closed-loop BWB aircraft model is stable and controllable before stall at $\alpha \approx 15°$. Therefore, a gradual nose-up maneuver is performed at about 30m/s while keeping the wing at level as shown in Fig. 10. At the beginning, the BWB model is stabilized by the CAS. Since the signal of ϕ is fed back to the controller, minor negative roll is observed. During about 3s to 14s, the pilot pushes the stick and the aircraft model nosed down from $\alpha \approx 5°$ to $\alpha \approx 2°$. Then, the pilot pulls the stick and the model nosed up gradually up to $\alpha \approx 11°$ at about 260s, while trying to maintain the wing at level and the sideslip at zero. During this time , a series of doublet maneuvers were applied to the q_{ref} to evaluate the performance of handing and tracking at different α. Rapid reference longitudinal tracking and negligible lateral/directional coupling are rated from the comments of the pilot. One can note that the maximum α reached about 14 °which is close to the boundary of stall. Compared to the surface deflection range listed in Table. 2, the required elevator deflections are moderate and far from the saturation. Hence, the designed CAS is valid to stabilize the BWB aircraft and improve the closed-loop handling performance throughout the attainable α before stall.

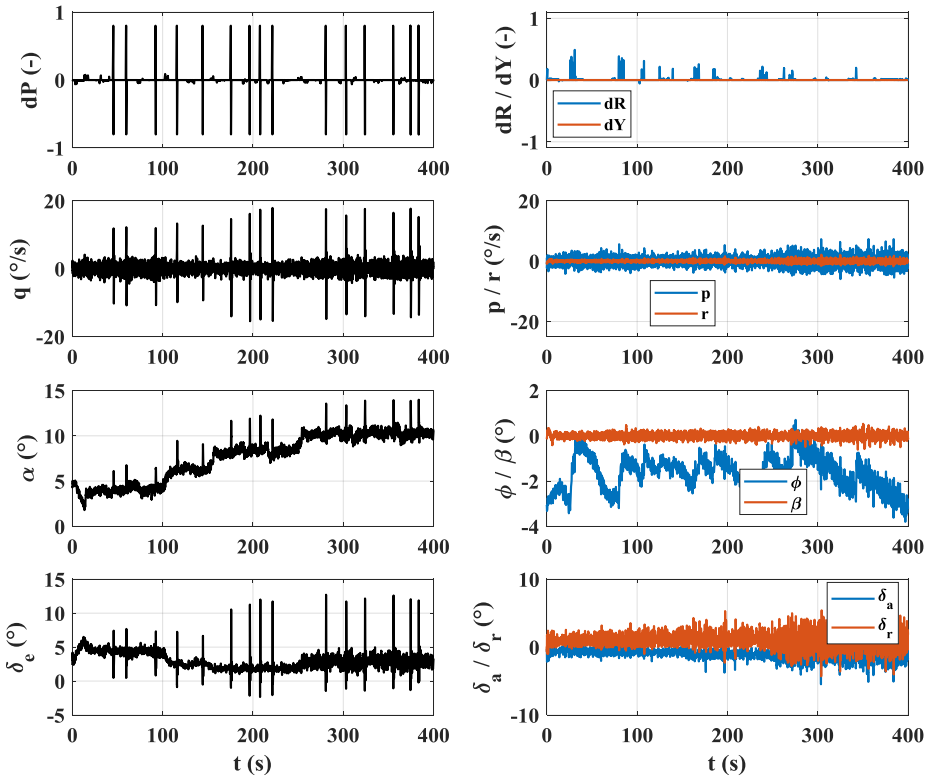

Figure 10 – Pilot steering and evaluation throughout the attainable α range.

4.2.2 Standard Reference Tracking and Evaluation

To evaluate the closed-loop performance in quantity, standard maneuver signals, such as the doublet, "3-2-1-1" and chirp waves, are usually applied to the reference inputs to the CAS. In this study, the doublets are applied to the longitudinal, lateral and directional channel respectively at different α. As demonstrated in Fig. 11, the BWB model is held at $\alpha \approx 10°$ by the CAS and disturbed with doublet for pitch, roll and yaw maneuver at the time of about 3s, 7s and 35s respectively. It is

observed that the actual responses of q, p and β are explicit and sufficient to demonstrate the capability of the designed CAS. Noticeable coupling between the lateral and directional channels is favorable for coordinated turns.

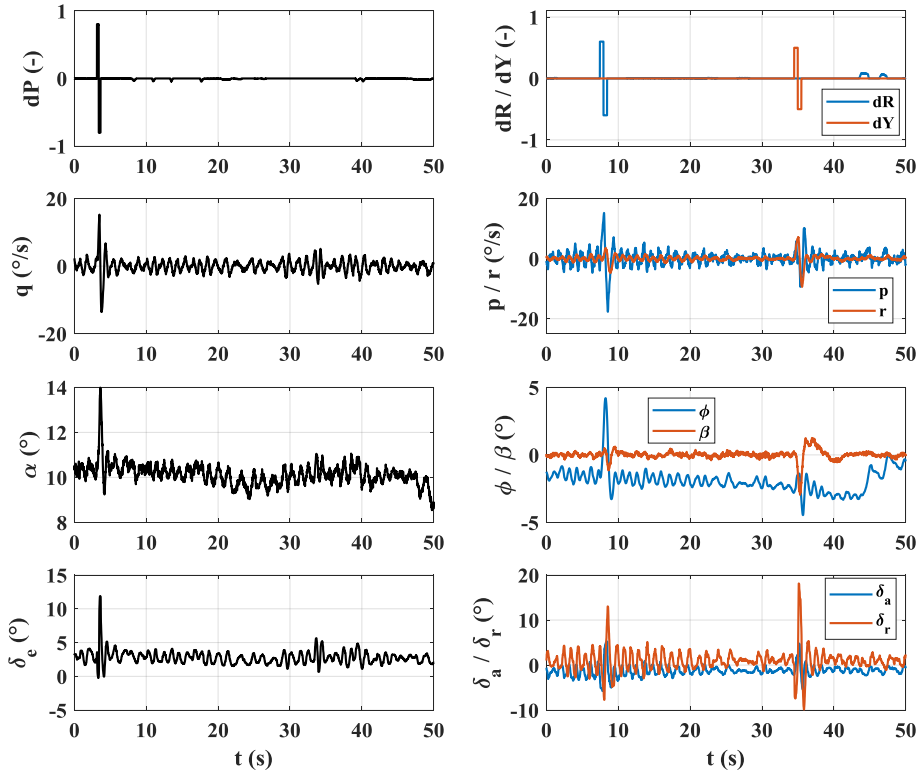

Figure 11 – Standard doublet reference tracking at $\alpha \approx 10°$.

The time history of pilot stick(d_P, d_R, d_Y), angular rate, attitude and surface deflections are acquired and recorded in real-time for offline identification. The technique of low-order-equivalent system(LOES) as illustrated in ref.[15] is employed to evaluate the closed-loop flying qualities. As aforementioned, the BWB aircraft suffer from the lack of conventional Dutch-roll characteristics, the closed-loop lateral/directional modal parameters are identified and plotted in Fig.12. Compared with the scaled criteria of the flying qualities in ref. [16,17], the Dutch-roll mode of the closed-loop BWB aircraft can be improved to Level 1 at low α for the three airframe configurations(*cfg1*: $\delta_{r0} = 0^\circ, \delta_{wt} = 0^\circ$; *cfg2*: $\delta_{r0} = 12^\circ, \delta_{wt} = 0^\circ$; *cfg3*: $\delta_{r0} = 0^\circ, \delta_{wt} = -40^\circ$). However, insufficient natural frequency and damping, resulting from the adverse decrease of the rudder effects with respect to the increase of α, is to be addressed in the future.

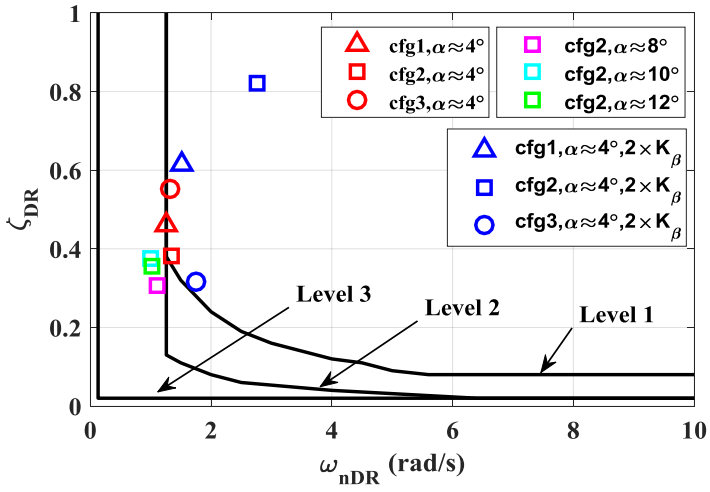

Figure 12 – Directional flying qualities of the closed-loop system.

5. Conclusion

Virtual flight tests have been performed for a sub-scaled BWB aircraft to validate the modeling and control law design in this paper. The mathematical model is derived according to the flight mechanics and constructed based on the conventional wind tunnel tests. The gain-scheduled CAS is employed to address the issues of significant change of the open-loop dynamics with alpha and adverse corruption of the Dutch-roll mode due to the lack of vertical tail. Successful virtual flights are carried out throughout the low to high alpha before stall, and good handling and flying qualities are obtained from the pilot rating and the results of LOES evaluation.

6. Contact Author Email Address

Mailto: liuzhitao@cardc.cn

7. Copyright Statement

References

[1] Hasan, Yasim J. und Schwithal, Jana und Pfeiffer, Till und Liersch, Carsten M. und Looye, Gertjan. Handling Qualities Assessment of a Blended Wing Body Configuration Under Uncertainty Considerations. Deutscher Luft- und Raumfahrtkongress, 2017, 05.-07. Sep. 2017, München, Deutschland.

[2] Dmitriev, V. G., Shkadov, L. M., Denisov, V. E., and Gurevich, B. I. The Flying-Wing Concept Chances and Risks. *AIAA/ICAS International Air and Space Symposium and Exposition: The Next 100 Years, Dayton, Ohio*, July 2003.

[3] Liebeck, R. H. Design of the Blended Wing Body Subsonic Transport. *Journal of Aircraft*, vol. 41, January - February 2004.

[4] Clark, L. R. and Gerhold, C. H. Inlet Noise Reduction by Shielding for the Blended-Wing-Body Airplane. *5th AIAA/CEAS Aeroacoustics Conference, Greater Seattle. Washington*, no. AIAA-99-1937, May 1999.

[5] Graham, W. R., Hall, C. A., and Vera Morales, M. The potential of future aircraft technology for noise and pollutant emissions reduction. *Elsevier, Transport Policy 34*, July 2014.

[6] Bowlus, J.; Multhopp, D.; Banda, S.; Bowlus, J.; Multhopp, D.; Banda, S. Challenges and opportunities in tailless aircraft stability and control. In Proceedings of the Guidance, Navigation, and Control Conference; American Institute of Aeronautics and Astronautics: Reston, VA, USA, 1997; pp. 1713–1718.

[7] Cook, M.V.; Castro, H. V The longitudinal flying qualities of a blended-wing-body civil transport aircraft. *Aeronaut. J.* 2004, *108*, 75–84, doi:10.1017/S0001924000005029.

[8] Voskuijl, M., La Rocca, G., and Dircken, F. Controllability of Blended Wing Body Aircraft. *ICAS, 26th International Congress of the Aeronautical Sciences, Anchorage, Alaska, USA*, September 2008.

[9] Kozek M , Schirrer A . Modeling and Control for a Blended Wing Body Aircraft: A Case Study. Advances in Industrial Control, 2015.

[10] D. D. Vicroy. Blended-Wing-Body low-speed flight dynamics: Summary of ground tests and sample results (Invited). 47th AIAA Aerospace Sciences Meeting including the New Horizons Forum and Aerospace Exposition, 2009.

[11]Stenfelt, G.; Ringertz, U. Yaw departure and recovery of a tailless aircraft configuration. *J. Aircr.* 2013, *50*, 311–315, doi:10.2514/1.C031868.

[12]Stenfelt, G.; Ringertz, U. Yaw control of a tailless aircraft configuration. *J. Aircr.* 2010, *47*, 1807–1811, doi:10.2514/1.C031017.

[13]L. Guo, M. Zhu, B. Nie, P. Kong, and C. Zhong. Initial virtual flight test for a dynamically similar aircraft model with control augmentation system. *Chinese J. Aeronaut.*, 2017.

[14]Stevens, B.L.; Lewis, F.L. *Aircraft Control. and Simulation*; 2004.

[15]Nie, B.; Liu, Z.; Cen, F.; Liu, D.; Ma, H.; Sename, O. An Innovative Experimental Approach to Lateral-Directional Flying Quality Investigation for Tailless Aircraft. *IEEE Access* 2020, *8*, 109543–109556, doi:10.1109/ACCESS.2020.3001913.

[16]Various, “Flying Qualities of Piloted Aircraft MIL-STD-1797A,” 1997.

[17][MIL-F-8785C, “Flying Qualities of Piloted Airplanes,” *United States Dep. Def.*, 1980.